Biophysical Journal Volume 82 April 2002 2005–2015

Ca^{2+}-Activated K^+ Currents Regulate Odor Adaptation by Modulating Spike Encoding of Olfactory Receptor Cells

Fusao Kawai

Department of Physiology, Fujita Health University, Toyoake, Aichi, 470-1192, Japan; and Department of Information Physiology, National Institute for Physiological Sciences, Myodaiji, Okazaki, Aichi, 444-8585, Japan

ABSTRACT The olfactory system is thought to accomplish odor adaptation through the ciliary transduction machinery in olfactory receptor cells (ORCs). However, ORCs that have lost their cilia can exhibit spike frequency accommodation in which the action potential frequency decreases with time despite a steady depolarizing stimulus. This raises the possibility that somatic ionic channels in ORCs might serve for odor adaptation at the level of spike encoding, because spiking responses in ORCs encode the odor information. Here I investigate the adaptational mechanism at the somatic membrane using conventional and dynamic patch-clamp recording techniques, which enable the ciliary mechanism to be bypassed. A conditioning stimulus with an odorant-induced current markedly shifted the response range of action potentials induced by the same test stimulus to higher concentrations of the odorant, indicating odor adaptation. This effect was inhibited by charybdotoxin and iberiotoxin, Ca^{2+}-activated K^+ channel blockers, suggesting that somatic Ca^{2+}-activated K^+ currents regulate odor adaptation by modulating spike encoding. I conclude that not only the ciliary machinery but also the somatic membrane currents are crucial to odor adaptation.

INTRODUCTION

A striking feature of the olfactory system is its ability to adapt to steady odor stimulation and to function over an enormous range of odor intensities (10^{-2}–10^{-10} mg/l; Amerine, 1965). The olfactory system is thought to accomplish odor adaptation through the ciliary transduction machinery in olfactory receptor cells (ORCs; Nakamura and Gold, 1987; Bakalyar and Reed, 1991; Breer and Boekhoff, 1992; Ronnett and Snyder, 1992; Firestein, 1992; Kleene, 1993; Kurahashi and Yau, 1994; Schild and Restrepo, 1998; Zufall and Leinders-Zufall, 2000). The initial step in olfactory sensation involves the binding of odorant molecules to specific receptor proteins on the ciliary surface of ORCs. Odorant receptors coupled to G proteins activate adenylyl cyclase leading to the generation of cAMP, which directly gates a cyclic nucleotide-gated (CNG) cationic channel in the ciliary membrane (Nakamura and Gold, 1987; Breer and Boekhoff, 1992; Firestein, 1992; Kleene, 1993; Kurahashi and Yau, 1994). Activation of the CNG channel allows an influx of Ca^{2+}, which is thought to mediate odor adaptation by desensitizing the CNG channel through which it entered the ORC. Desensitization is also mediated by calmodulin and possibly also by a Ca^{2+}-binding protein (Bakalyar and Reed, 1991; Kurahashi and Yau, 1994; Restrepo et al., 1996).

However, isolated ORCs that have lost their cilia are known to exhibit spike frequency "accommodation" in which the action potential frequency decreases with time despite a steady depolarizing stimulus (Kawai et al., 1999). This raises the possibility that somatic ionic channels in ORCs may serve for odor adaptation at the level of spike encoding, because spiking responses in ORCs encode the odor information (Frings and Lindemann, 1990; Trotier, 1994; Kawai et al., 1997; Duchamp-Viret et al., 1999; Kawai et al., 1999; Kawai and Miyachi, 2001). The sensory adaptation refers to a decrease in receptor sensitivity that occurs in the presence of a maintained stimulus or a conditioning stimulus (Torre et al., 1995). Because olfactory adaptation is defined as a shift of the dynamic response range due to conditioning stimuli (Torre et al., 1995; Kurahashi and Menini, 1997), to characterize spike frequency "adaptation," not "accommodation," of ORCs, effects of a first conditioning stimulus on the spiking response to a second test stimulus of the same intensity were examined in the present study.

I investigated selectively the adaptational mechanism at the somatic membrane using conventional and dynamic patch-clamp recording techniques, which enable the ciliary mechanism to be bypassed. First, using the conventional perforated patch-clamp recordings, I found that an influx of Ca^{2+} through the somatic membrane is involved in spike frequency adaptation in ORCs. Because the adaptational mechanism at the ciliary membrane is also regulated by Ca^{2+} influx (Bakalyar and Reed, 1991; Breer and Boekhoff, 1992; Ronnett and Snyder, 1992; Firestein, 1992; Kleene, 1993; Kurahashi and Yau, 1994; Schild and Restrepo, 1998), to bypass the Ca^{2+}-dependent adaptational mechanism at the ciliary membrane, the dynamic patch-clamp recording techniques were next used. First in a Ca^{2+}-free bath solution odorant-induced currents were recorded from intact ORCs under voltage-clamp conditions, and then in control Ringer's solution spiking responses to depolarization induced by injection of the same odorant-induced cur-

Submitted July 24, 2001, and accepted for publication December 28, 2001.

Address reprint requests to Dr. Fusao Kawai, Department of Physiology, School of Medicine, Fujita Health University, 1-98 Dengakugakubo, Kutsukakechou, Toyoake, Aichi, 470-1192, Japan. Tel.: 81-562-93-2466; Fax: 81-562-93-2649; E-mail: fkawai@fujita-hu.ac.jp.

0006-3495/02/04/2005/11 $2.00

rents were examined under current-clamp conditions. I discovered that odorant stimuli (amyl acetate) can induce the spike frequency adaptation in intact ORCs through somatic Ca^{2+}-activated K^+ currents.

MATERIALS AND METHODS

Preparation and recording procedures

ORCs were dissociated enzymatically from the olfactory epithelium of the newt, *Cynops pyrrhogaster* as reported (Kurahashi and Kaneko, 1993; Kawai et al., 1996). Isolated cells were viewed on an Olympus upright microscope (Tokyo, Japan) with differential interference contrast optics (40× water-immersion objective). To examine the somatic membrane currents, ORCs were mainly selected that had lost their cilia except for the odorant stimulation experiments. Membrane voltages and currents were recorded in the β-escin perforated patch-clamp configuration (Fan and Palade, 1998) using a patch-clamp amplifier (Axopatch 200B, Axon Instruments, Foster City, CA) linked to a computer. Recording procedures were controlled by pCLAMP software (Axon Instruments). Data were low-pass filtered (4-pole Bessel type) with a cutoff frequency of 5 kHz and then digitized at 10 kHz by an analog-to-digital interface. In all current clamp experiments a holding current was 0 pA. In voltage clamp experiments the leak currents were subtracted. All experiments were done at room temperature (23–25°C).

Correction of the resting potential

ORCs show a high input resistance (>2 GΩ; Kawai et al., 1996; Schild and Restrepo, 1998), so a small leakage current causes an error in the recorded membrane potential. In the present study, therefore, the resting potential was corrected for by using the following equations, as reported previously (Kawai et al., 1996):

$$1/R_{inp} = 1/R_{mem} + 1/R_{seal}$$

$$(V_{ap} - V_{real})/R_{mem} + V_{ap}/R_{seal} = 0$$

in which R_{inp} is the input resistance, R_{mem} the membrane resistance, and R_{seal} the seal resistance. V_{ap} and V_{real} are the apparent and the real resting potential, respectively. V_{real} and R_{mem} were estimated from R_{inp}, R_{seal}, and V_{ap} recorded in the experiment. The resting potentials to be described below are the corrected values.

Solutions and odorant stimuli

The recording pipette was filled with pseudo-intracellular (K^+) solution (119 mM KCl, 1 mM $CaCl_2$, 5 mM EGTA, 10 mM HEPES, and 50 μM β-escin, pH adjusted to 7.4 with KOH). β-escin was prepared daily or as a 50 mM stock solution in water or stored up to one week at −20°C (Fan and Palade, 1998). The resistance of the pipette was ~6 MΩ. The control extracellular solution used to record voltage responses contained: 110 mM NaCl, 3.7 mM KCl, 3 mM $CaCl_2$, 2 mM HEPES, and 15 mM glucose, the Ca^{2+}-free bath solution used to record odorant-induced currents contained 115 mM NaCl, 3.7 mM KCl, 2 mM HEPES, and 15 mM glucose, and the solution for outward K^+ currents contained 110 mM choline-Cl, 3.7 mM KCl, 3 mM $CaCl_2$, 2 mM HEPES, and 15 mM glucose. For odorant stimuli, amyl acetate (100 μM) was dissolved in a bath solution, included into a puffer pipette, and applied from a pressure ejection system. All test drugs (charybdotoxin, iberiotoxin, apamine, 4-acetamido-4′-isothiocyanatostilbene-2, 2′-disulfonic acid [SITS], $CoCl_2$, and CsCl) were purchased from Sigma (St. Louis, MO) and applied to the bath solution.

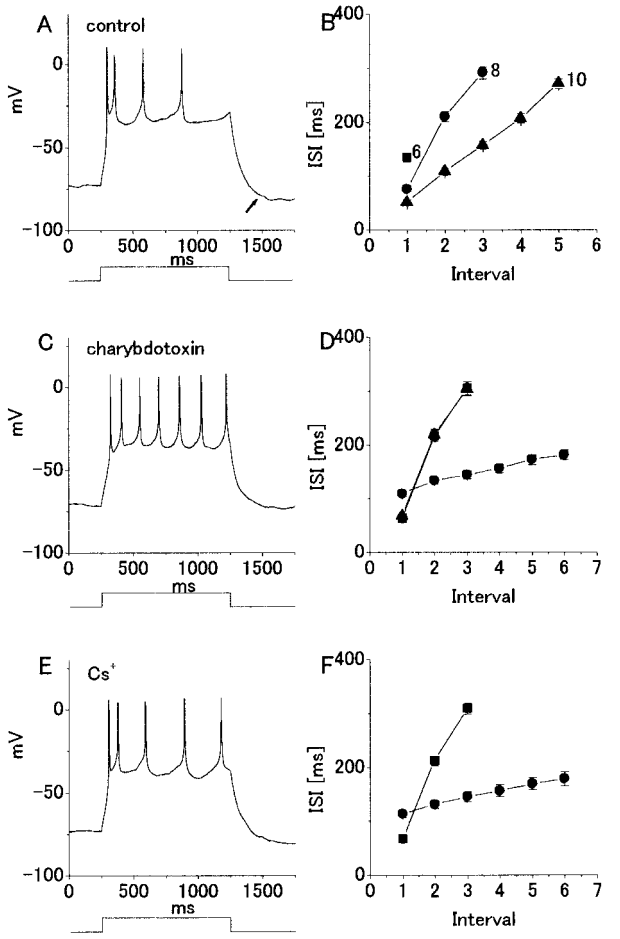

FIGURE 1 Spike frequency accommodation of an isolated ORC. (*A*, *C*, and *E*) Action potentials in response to +8 pA depolarizing current injection in control Ringer's solution (*A*), 100 nM charybdotoxin (*C*), or 2 mM CsCl (*E*). Each voltage response was recorded from the same cell using the β-escin perforated patch-clamp technique. (*B*) Interspike interval (ISI) versus interval number plots were generated in response to 1-s depolarizing current steps of 6 pA (■), 8 pA (●), and 10 pA (▲) in control Ringer's solution. Current intensities are labeled for each plot. Each symbol represents the mean of seven cells ± standard error. (*D*) ISI versus interval number plots in response to +8 pA current step in control (■, n = 7), 100 nM charybdotoxin (●, n = 7), or 2 mM CsCl (▲, n = 4). (*F*) ISI versus interval number plots in response to +8 pA current step in control (■, n = 7) or 50 nM iberiotoxin (●, n = 4).

RESULTS

Spike frequency accommodation of an isolated olfactory receptor cell

To investigate selectively the effects of somatic membrane currents in ORCs on odor adaptation, isolated ORCs that had lost their cilia were chosen. Using the conventional perforated patch-clamp technique (Fan and Palade, 1998), the firing properties of ORCs in response to depolarizing current injections of varying intensities by plotting interspike intervals (ISI) versus interval number were examined (Fig. 1). The current amplitudes were chosen to correspond

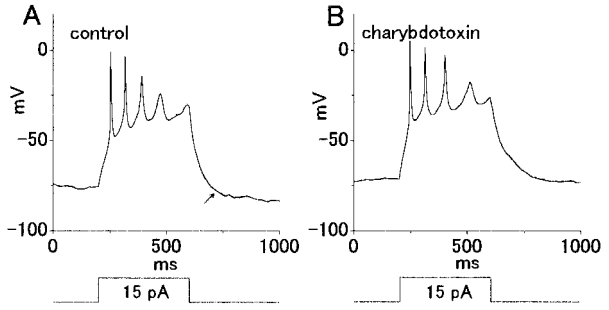

FIGURE 2 Spike frequency accommodation of an ORC at a high intensity of the current step. (*A* and *B*) Action potentials in response to +15 pA depolarizing current step in control Ringer's solution (*A*) or 100 nM charybdotoxin (*B*). Each voltage response was recorded from the same cell as in Fig. 1.

to ORC responses to a typical range of odor concentrations (Firestein et al., 1993; Kurahashi and Menini, 1997). In control Ringer's solution, injection of a +8 pA current step to an ORC induced four spikes, which exhibited a strong accommodating firing pattern (Fig. 1 *A*). When a +15 pA current step was injected into the same cell, a similar accommodating firing was also observed, however, the spike amplitude was progressively reduced (Fig. 2 *A*). After the termination of the depolarizing current step, a prominent after-hyperpolarization (AHP) was observed (arrows in Figs. 1 *A* and 2 *A*). As the current intensity was increased, the slope of the ISI relationship became less steep (Fig. 1 *B*; $n = 7$).

In central nervous system (CNS) neurons Ca^{2+}-activated K^+ currents are involved in spike frequency accommodation (Gorman and Thomas, 1978; Adams et al., 1980; Yarom et al., 1985; Hille, 1992; Fohlmeister and Miller, 1997; Chitwood and Jaffe, 1998), so the effects of somatic Ca^{2+}-activated K^+ currents on spiking responses of ORCs were examined. Under bath application of 100 nM charybdotoxin, a blocker of Ca^{2+}-activated K^+ channels of the big K (BK) type, the ORC fired trains of weakly accommodating action potentials, and the AHP was almost completely abolished (Fig. 1 *C*; $n = 7$). A similar result was obtained with the application of 50 nM iberiotoxin, a specific blocker of BK channels (Candia et al., 1992; Puro and Stuenkel, 1995; Kusaka et al., 1998; $n = 4$) and by 1 mM $CoCl_2$, a blocker of voltage-gated Ca^{2+} channels ($n = 4$). However, 100 nM apamine, a blocker of Ca^{2+}-activated K^+ channels of the small K (SK) type, was ineffective ($n = 5$). Application of 100 nM charybdotoxin also made the slope of the ISI relationship less steep (Fig. 1 *D*, filled circles). The first ISI in charybdotoxin was longer than that under control conditions (Fig. 1 *D*). A similar result was obtained by application of 50 nM iberiotoxin (Fig. 1 *F*, filled circles). These suggest that Ca^{2+}-activated K^+ currents of the BK type are responsible for spike frequency accommodation of ORCs. When a higher intensity (15 pA) of the current step was injected into the ORC, however, application of 100 nM charybdotoxin did not change the accommodating firing pattern significantly (Fig. 2 *B*). This suggests that some current other than the Ca^{2+}-activated K^+ currents is also involved in spike frequency accommodation in ORCs during injection of high intensity current steps.

Furthermore, I also tested the effects of a hyperpolarization-activated cationic current (*h* current) on spike frequency accommodation in ORCs, because the *h* current is also known to be involved in spike frequency accommodation in CNS neurons (McCormick and Pape, 1990; Womble and Moises, 1993; Chitwood and Jaffe, 1998). Bath application of 2 mM CsCl, a blocker of *h* current, did not markedly change the firing patterns (Fig. 1 *E*; $n = 4$) or the ISI relationship (Fig. 1 *D*, filled triangles), suggesting that *h* currents are not involved in spike frequency accommodation of newt ORCs.

Spike frequency adaptation of an ORC

Because olfactory adaptation is defined as a shift of the dynamic response range due to conditioning stimuli (Torre et al., 1995; Kurahashi and Menini, 1997), I investigated effects of the first conditioning current pulse on the spiking response to the second test current pulse of the same intensity and duration (Fig. 3 *A*). The first pulse induced five spikes, and the second pulse three spikes. Thus the ORC exhibits spike frequency adaptation. An AHP was observed in the first and the second responses (arrows in Fig. 3 *A*). The shift of the dynamic range induced by the conditioning pulse was clearly observed in the spiking responses of 0.5-s interpulse interval (Fig. 3 *C*, filled triangles). The first conditioning current pulse was the same intensity and duration as the second test current pulse. In the presence of the conditioning pulse, a higher intensity of current was required to generate a spiking response of the same frequency. The dynamic range of the second pulse recovered as the interpulse interval increased (interval = 3 s; Fig. 3 *C*, filled squares). Stimuli at high intensities (more than 12 pA) progressively reduced spike frequency (Fig. 3 *C*), probably due to inactivation of voltage-gated Na^+ currents during the maintained depolarization (see Discussion).

When double pulse experiments were repeated in the bath containing 100 nM charybdotoxin, the AHP was reversibly blocked and there was no significant difference between the first and second responses to current injections (Fig. 3 *B*). The dynamic range of the test pulse was almost equal to that of the conditioning pulse (Fig. 3 *D*; $n = 7$). A similar result was obtained after the addition of 50 nM iberiotoxin ($n = 4$) and 1 mM $CoCl_2$ ($n = 4$), indicating that Ca^{2+}-activated K^+ currents are responsible for spike frequency adaptation. By contrast, 2 mM CsCl was ineffective ($n = 4$), indicating that *h* currents are not responsible for spike frequency adaptation. These results suggest that the somatic Ca^{2+}-activated

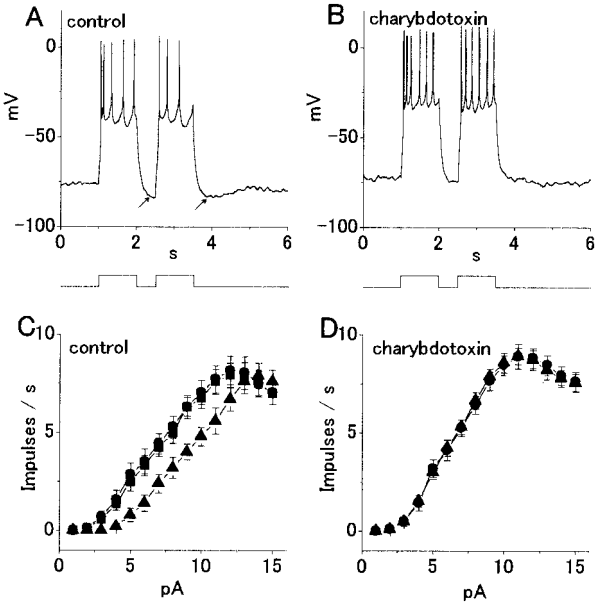

FIGURE 3 Spike frequency adaptation of an ORC. (*A*) Spiking response to depolarization induced by current injection in control Ringer's solution. Two current pulses of the same amplitude (8 pA) and duration (1 s) were applied to an isolated ORC at the interval of 0.5 s. (*B*) Response to the same depolarization, recorded from the same cell as in *A*, after addition of 100 nM charybdotoxin. (*C*) The relationship between current intensity and spike frequency of the first (●) and second (▲ and ■) depolarizations in control Ringer's solution. The first conditioning current pulse was the same intensity and duration (1 s) as the second test pulse. Filled triangles and squares show the interpulse intervals of 0.5 s and 3 s, respectively. Each symbol represents the mean of seven cells ± standard error. (*D*) Relationship between current intensity and spike frequency of the first (●) and second (▲) depolarizations in the presence of 100 nM charybdotoxin. The first current pulse was the same intensity and duration (1 s) as the second pulse. The interpulse interval was 0.5 s.

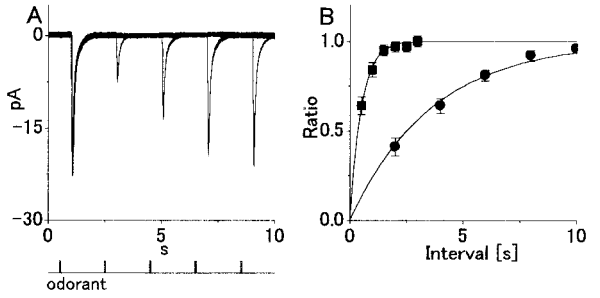

FIGURE 4 Comparison of the kinetics of the recovery from adaptation between spike frequency and an odorant-induced current. (*A*) The odorant-induced current with leak current subtracted was recorded from an intact ORC with its cilia attached in control Ringer's solution (holding potential, $V_h = -70$ mV). Double pulses of the odorant amyl acetate at the same concentration (100 μM) and duration (50 ms) were applied to the cell at intervals of 2, 4, 6, and 8 s. Timing of odorant stimulation is indicated by the upward deflection shown below the current traces. (*B*) Time course of the recovery from odorant-induced current adaptation (●) and spike frequency adaptation (■). Each symbol represents the mean ± standard error. To examine the recovery from spike frequency adaptation, a first current step was applied to an ORC and followed by a second pulse of the same intensity (8 pA) and duration (1 s). In both the odorant-induced current adaptation and spike frequency adaptation, the ratio values of the response to the test pulse to the response to the conditioning pulse were plotted versus the interpulse interval. The intervals for spike frequency are 0.5, 1, 1.5, 2, 2.5, and 3 s, and the intervals for the odorant-induced current 2, 4, 6, 8, and 10 s. Each datum was fitted by a single exponential function (1 - [exp(-1 × t/τ)]) in which t is the interval between the pulse, and τ is the time constant of recovery, estimated at 0.51 s (■, $n = 7$) and at 3.7 s (●, $n = 5$).

K^+ currents may regulate odor adaptation by modulating spike encoding in ORCs.

Kinetics of the recovery from adaptation

To compare the kinetics of the recovery from spike frequency adaptation with that from odorant-induced ciliary current adaptation, an odorant-induced current was recorded. An odor pulse (amyl acetate) was applied to an intact ORC and followed by a second pulse of the same intensity and duration (Fig. 4 *A*). The peak amplitude of the response to the second pulse was smaller for short interpulse intervals but recovered as the interpulse intervals increased. A similar result is reported previously (Kurahashi and Menini, 1997). The time course of the recovery of the odorant-induced current could be fitted by a single exponential function with a time constant of 3.7 s (Fig. 4 *B*, filled circles).

The kinetics of the recovery from spike frequency adaptation was also investigated (Fig. 4 *B*, filled squares). A first current step was applied to an ORC and followed by a second pulse of the same intensity and duration. In Fig. 4 *B* (filled squares), the ratio of the number of the spiking response to the test pulse to that to the conditioning pulse was plotted versus the interpulse interval. The time course of the recovery from spike frequency adaptation could also be fitted by a single exponential function with a time constant of 0.51 s (Fig. 4 *B*, filled squares), which is much smaller than the time constant of the odorant-induced current (3.7 s). Thus, the spike frequency of ORCs recovers from adaptation more rapidly than the odorant-induced current.

Odor adaptation at the level of action potentials

Because the adaptational mechanism at the ciliary membrane as well as at the somatic membrane is regulated by an influx of Ca^{2+} (Bakalyar and Reed, 1991; Breer and Boekhoff, 1992; Ronnett and Snyder, 1992; Firestein, 1992; Kleene, 1993; Kurahashi and Yau, 1994; Kurahashi and Menini, 1997), it is still unclear, however, whether odorant stimuli can induce spike frequency adaptation in intact ORCs through the somatic Ca^{2+}-activated K^+ currents. To examine this, the dynamic patch-clamp recording technique was used. First, in Ca^{2+}-free bath solution odorant-induced currents were recorded from intact ORCs under voltage-

clamp conditions, and then in control Ringer's solution spiking responses to depolarization induced by injection of the same odorant-induced currents were examined under current-clamp conditions. When double odorant pulses (amyl acetate) of the same concentration and duration were applied to an intact ORC in Ca^{2+}-free bath solution, there was no significant difference between the first and second current responses to odorant pulses at all interpulse intervals of 1, 2, and 3 s (Fig. 5 *A*).

Injection of the same odorant-induced current, which was recorded under voltage-clamp conditions (Fig. 5 *A*), induced spike frequency adaptation in the intact ORC (Fig. 5 *B*). In control Ringer's solution the first depolarization induced three spikes, and the second depolarization at the interval of 1 s induced two spikes. An AHP was observed in both responses (arrows in Fig. 5 *B*). The shift of the dynamic range induced by the conditioning odorant-induced current was clearly observed in the spiking responses at the interval of 1 s (Fig. 5 *E*, filled triangles). In contrast, there was no significant difference between the first and second response at the interval of 3 s (Fig. 5 *C*) and also no difference in the dynamic range (Fig. 5 *E*, filled squares).

When the same experiment was repeated in the bath containing 100 nM charybdotoxin, the AHP was blocked and there was no significant difference between the first and second spiking responses to the odorant-induced currents (Fig. 5 *D*). Furthermore, the dynamic range of the spiking responses to the test stimulus was almost equal to that of the conditioning stimulus (Fig. 5 *F*; $n = 6$). A similar result was obtained by application of 50 nM iberiotoxin ($n = 4$). These results suggest that odorant stimuli induce odor adaptation in intact ORCs through the somatic Ca^{2+}-activated K^+ currents.

Furthermore, I directly measured spike frequency adaptation in response to real odor pulses with the cell current clamped. In control Ringer's solution the first odorant pulse induced three spikes, and the second pulse at the interval of 1 s induced no spike (Fig. 6A). Although the spiking response to the first odorant pulse in Fig. 6 *A* was similar to that in Fig. 5 *B*, the response to the second pulse in Fig. 6 *A* was quite different from that in Fig. 5 *B*. In Fig. 5 *B*, the second pulse induced two spikes. This difference can be explained by the difference between the amplitude of the transduction current induced by the first odorant pulse and that by the second pulse (see Fig. 4 *A*). That is, in control Ringer's solution the amplitude of the transduction current induced by the first pulse was much larger than the current induced by the second pulse at the interval of 2 s. In contrast, in Ca^{2+}-free bath solution (Fig. 5 *B*) the same amplitude of the transduction current was injected into the cell at all intervals.

After the interval of 3 s the second odorant pulse induced a single spike (Fig. 6 *B*). This spiking response was also different from the response to the second pulse in Ca^{2+}-free bath solution (Fig. 5 *C*). In Fig. 5 *C*, the second pulse induced three spikes. This difference can also be explained by the difference of the amplitude of the transduction current.

Compared with Fig. 6 *A*, bath application of iberiotoxin increased the spike number of the response to the second odorant pulse (Fig. 6 *C*). In the presence of 50 nM iberio-

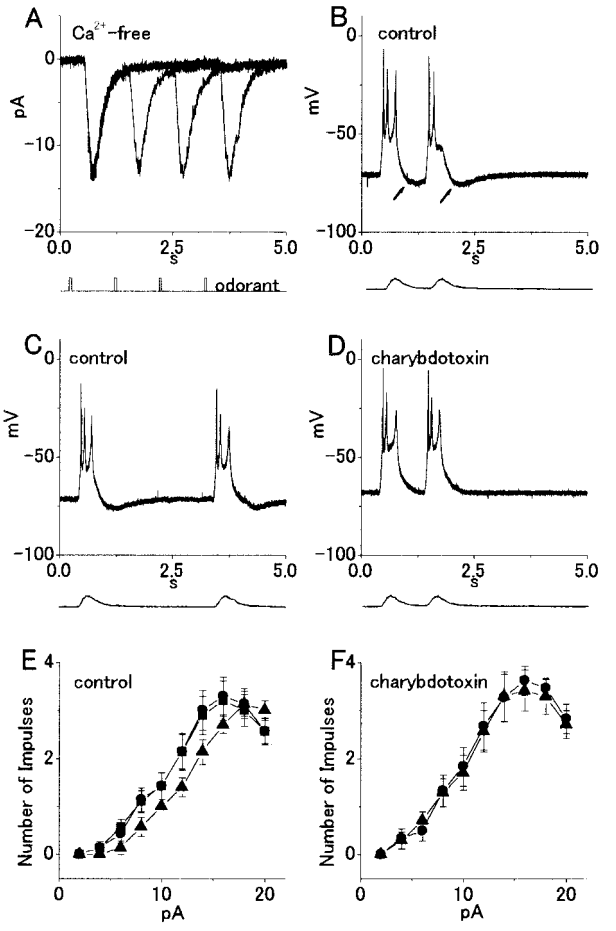

FIGURE 5 Odor adaptation at the level of action potentials. (*A*) Odorant-induced currents with leak current subtracted was recorded from an intact ORC with its cilia attached in a Ca^{2+}-free bath solution ($V_h = -70$ mV). Double pulses of the odorant amyl acetate at the same concentration (100 μM) and duration (50 ms) were applied to the cell at intervals of 1, 2, and 3 s. Timing of odorant stimulation is indicated by the upward deflection shown below the current traces. (*B* and *C*) Spiking responses to depolarization induced by injection of the same odorant-induced current traces as in *A* at intervals of 1 s (*B*) and 3 s (*C*) in control Ringer's solution under current-clamp conditions. Each odorant-induced current trace is shown below the voltage response. (*D*) Spiking responses to depolarization induced by injection of the same current as in (*A*, interval = 1 s) in the bath solution containing 100 nM charybdotoxin. (*E*) The relationship between odorant-induced current and spike number of the response to the first (●) and second (▲ and ■) depolarizations in control Ringer's solution. Filled triangles and squares show the intervals of 1 s and 3 s, respectively. Each symbol represents the mean of six cells ± standard error. (*F*) Relationship between odorant-induced current and spike number of the response to the first (●) and second (▲) depolarizations in the presence of 100 nM charybdotoxin. The interval of the odorant-induced current was 1 s.

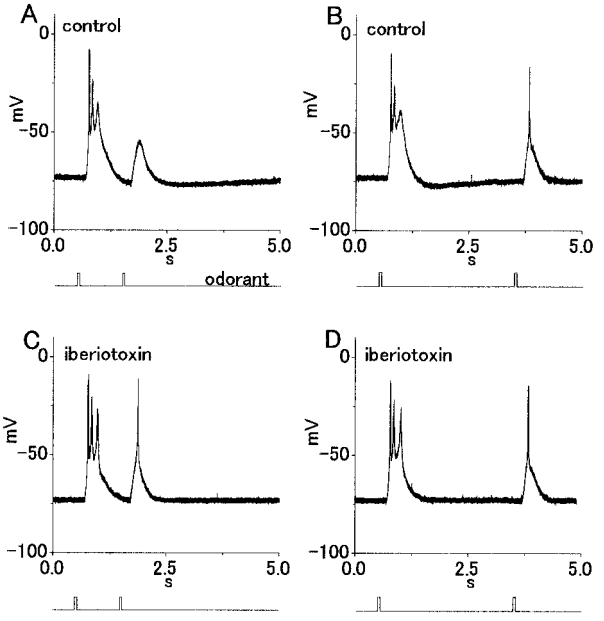

FIGURE 6 Spike frequency adaptation in response to real odor pulses with an ORC current clamped. (*A* and *B*) Spiking responses to odorant pulses in control Ringer's solution. Double pulses of the odorant amyl acetate at the same concentration (100 μM) and duration (50 ms) were applied to the cell at intervals of 1 s (*A*) and 3 s (*B*). Timing of odorant stimulation is indicated by the upward deflection shown below the voltage traces. (*C* and *D*) Spiking responses to double pulses of the odorant in the bath containing 50 nM iberiotoxin. The voltage responses were recorded from the same cell as in *A* and *B*. The odorant pulses were applied to the cell at intervals of 1 s (*C*) and 3 s (*D*).

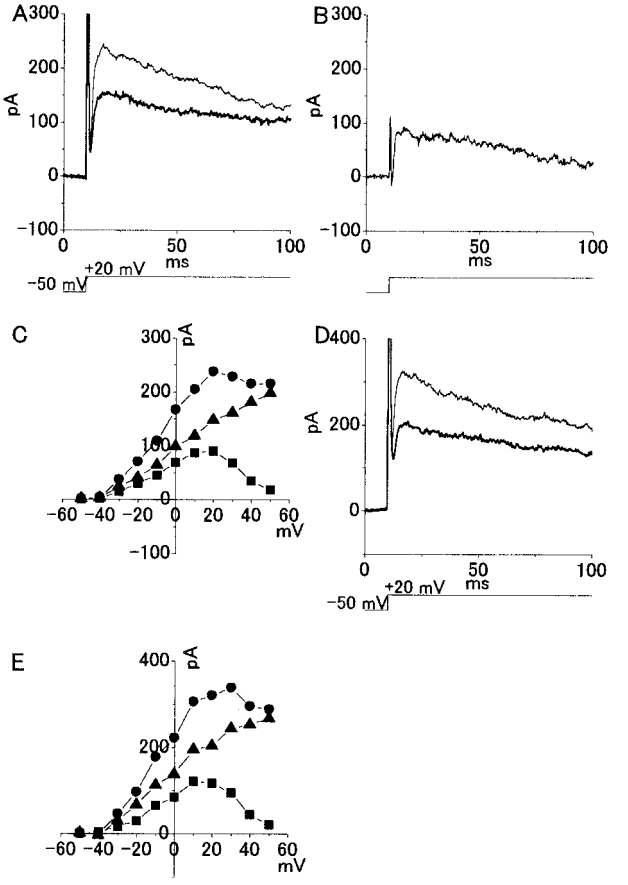

FIGURE 7 Charybdotoxin and iberiotoxin block Ca^{2+}-activated K^+ currents in ORCs. (*A*) Outward currents with leak current subtracted were induced by depolarization to +20 mV (V_h = −50 mV) in control Na^+-free solution (*thin line*) and 100 nM charybdotoxin (*thick line*). (*B*) Ca^{2+}-activated K^+ currents (charybdotoxin-sensitive currents) obtained by subtracting the thick line from the thin line in *A*. (*C*) I-V relationship of the cell shown in *A*. Peak outward currents in control solution (●), 100 nM charybdotoxin (▲), and of their subtraction (■) were plotted against test-pulse voltage. (*D*) Outward currents with leak current subtracted were induced by depolarization to +20 mV (V_h = −50 mV) in control Na^+-free solution (*thin line*) and 50 nM iberiotoxin (*thick line*). (*E*) I-V relationship of the cell shown in *D*. Peak outward currents in control solution (●), 50 nM iberiotoxin (▲), and of their subtraction (■) were plotted against test-pulse voltage.

toxin the second pulse at the interval of 1 s induced a single spike (Fig. 6 *C*), whereas in control Ringer's solution the second pulse induced no spike (Fig. 6 *A*). Because it is unlikely that iberiotoxin affects directly the transduction current, the single spike induced by the second pulse in Fig. 6 *C* is caused by a reduction of Ca^{2+}-activated K^+ currents rather than an increase of the transduction current during the second pulse. In contrast, application of iberiotoxin did not change the spike number of the response to the second odorant pulse of 3-s interval (Fig. 6 *D*). Both second pulses in control Ringer's solution (Fig. 6 *B*) and the solution containing 50 nM iberiotoxin (Fig. 6 *D*) induced a single spike. These results suggest that the somatic adaptational mechanism through the Ca^{2+}-activated K^+ currents contributes to odor adaptation only for a short period (~1 s) compared with the ciliary adaptational mechanism.

ORCs express Ca^{2+}-activated K^+ currents

To confirm whether newt ORCs really express Ca^{2+}-activated K^+ currents, I examined their membrane currents. Outward currents induced by membrane depolarization were reduced by bath application of 100 nM charybdotoxin (Fig. 7 *A*; n = 4). A similar result was obtained by bath application of 50 nM iberiotoxin (Fig. 7 *D*; n = 4) and 1 mM $CoCl_2$ (n = 16), but 100 nM apamine was ineffective (n = 5). The membrane current in the presence of charybdotoxin from normal record was subtracted to reveal the Ca^{2+}-activated K^+ current (Fig. 7 *B*). This current began to be activated at −30 mV and was at the maximum at +20 mV (Fig. 7 *C*, filled squares), which was similar to the voltage dependence of L-type Ca^{2+} currents in ORCs (Firestein and Werblin, 1987; Maue and Dionne, 1987; Schild, 1989; Miyamoto et al., 1992; Nevitt and Moody, 1992; Kawai et al., 1996; Lucero and Chen, 1997). A similar I-V relationship was obtained by bath application of 50 nM

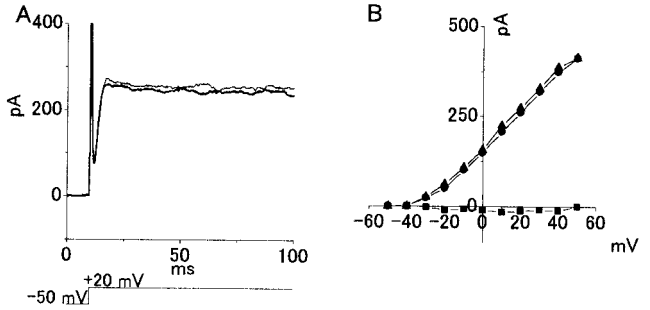

FIGURE 8 Effects of an influx of Ca^{2+} on voltage-gated K^+ currents in the presence of 50 nM iberiotoxin. (*A*) Outward currents with leak current subtracted were induced by depolarization to +20 mV (V_h = −50 mV) in control solution (*thin line*) and Ca^{2+}-free solution (*thick line*). The Ca^{2+}-free solution contained 3 mM $CoCl_2$. To block BK channels 50 nM iberiotoxin was added to the bath. (*B*) I-V relationship of the cell shown in *A*. Peak currents in control solution (●), Ca^{2+}-free solution (▲), and of their subtraction (■) were plotted against test-pulse voltage.

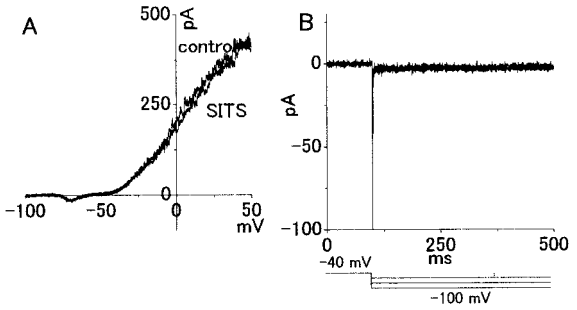

FIGURE 9 Newt ORCs do not express Ca^{2+}-activated Cl^- channels or *h* channels in their somatic membrane. (*A*) Effects of 2 mM SITS on I-V relationship. The cell was voltage clamped at −100 mV and a ramp depolarization was applied at a speed of 100 mV/s under control conditions and in the presence of 2 mM SITS. The leak current was subtracted. (*B*) Hyperpolarizing voltage steps from a V_h of −40 mV did not induce membrane currents. Command voltages were increased in 20 mV steps from −100 mV to −60 mV. The leak current was subtracted.

iberiotoxin (Fig. 7 *E*). These suggest that newt ORCs express Ca^{2+}-activated K^+ channels of the BK type.

In retinal glial cells, Kusaka et al. (1998) report that an influx of Ca^{2+} modulates voltage-gated K^+ channels (K_V1.3 channels). To test whether an influx of Ca^{2+} also affects voltage-gated K^+ currents in newt ORCs, its effects were examined in presence of 50 nM iberiotoxin. However, there was little difference between the voltage-gated K^+ currents in the presence or absence of external Ca^{2+} (Fig. 8 *A*; n = 5). In the Ca^{2+}-free solution Co^{2+} was substituted for Ca^{2+}. The difference between the I-V curves in the presence or absence of external Ca^{2+} (Fig. 8 *B*, filled squares) was similar to the voltage dependence of L-type Ca^{2+} currents (Kawai et al., 1996), but was quite different from that of voltage-gated K^+ currents. Thus, an influx of Ca^{2+} through voltage-gated Ca^{2+} currents does not significantly modulate voltage-gated K^+ channels in newt ORCs. In contrast, as shown above, in the absence of iberiotoxin bath application of 1 mM $CoCl_2$ markedly reduced the outward current induced by membrane depolarization. Thus, Co^{2+} decreases Ca^{2+}-activated K^+ currents by inhibiting an influx of Ca^{2+} through voltage-gated Ca^{2+} channels.

In addition, I examined whether the ORCs express other Ca^{2+}-activated channels such as Ca^{2+}-activated Cl^- channels in their somatic membrane. However, the I-V relation obtained in the solution containing 2 mM SITS, a Ca^{2+}-activated Cl^- channel blocker, was almost identical to that obtained in the control solution (Fig. 9 *A*; n = 6), suggesting that the ORCs do not express Ca^{2+}-activated Cl^- channels in their somatic membrane. Furthermore, I also examined whether the ORCs have *h* currents. Hyperpolarizing voltage steps from a holding potential of −40 mV failed to induce membrane currents (Fig. 9 *B*). A similar result was obtained in all recorded ORCs (n = 85), suggesting that newt ORCs do not express *h* currents.

DISCUSSION

Ca^{2+}-activated K^+ currents in ORCs

Ca^{2+}-activated K^+ currents are found in ORCs from various species (squid, Lucero and Chen, 1997; lobster, Corotto and Michel, 1998; salmon, Nevitt and Moody, 1992; zebrafish, Corotto et al., 1996; toad, Delgado and Labarca, 1993; salamander, Trotier, 1986; *Xenopus laevis* frogs, Schild, 1989; mouse, Maue and Dionne, 1987). A fraction of the outward current in *Xenopus* ORCs is blockable by apamine (Schild, 1989), which blocks Ca^{2+}-activated K^+ channels of the SK type. By contrast, in squid ORCs Ca^{2+}-activated K^+ currents are blocked by charybdotoxin but are insensitive to apamine (Lucero and Chen, 1997). In the present experiment outward currents in newt ORCs were blocked selectively by charybdotoxin but were insensitive to apamine. Because charybdotoxin is known to block not only Ca^{2+}-activated K^+ channels but also some voltage-gated K^+ channels (Kusaka et al., 1998), the effects of iberiotoxin, a specific blocker of BK channels, on the currents in newt ORCs were also examined. Iberiotoxin also blocked a fraction of the outward currents in the ORCs. These suggest that the ORCs express Ca^{2+}-activated K^+ channels of the BK type rather than the SK type.

In some CNS neurons, *h* currents are involved in the generation of AHP and spike frequency accommodation (McCormick and Pape, 1990; Hille, 1992; Womble and Moises, 1993). I examined whether newt ORCs also express *h* currents. However, hyperpolarizing voltage steps from a V_h of −40 mV induced no inward current in all ORCs recorded (n = 85), suggesting that newt ORCs do not express *h* currents. This is consistent with previous observations from various ORCs (*Manduca sexta*, Zufall et al., 1991; squid, Lucero and Chen, 1997; *Xenopus*, Schild, 1989; tiger salamander, Firestein and Werblin, 1987). By contrast, *h* currents are known to be expressed in ORCs of

some species (lobster, Corotto and Michel, 1998; catfish, Miyamoto et al., 1992; rat, Lynch and Barry, 1991). The presence of *h* currents in ORCs may depend on the species.

AHP and spike frequency accommodation in CNS neurons and ORCs

Many neurons in various preparations are known to exhibit spike frequency accommodation (Yarom et al., 1985; Fohlmeister and Miller, 1997; Chitwood and Jaffe, 1998; Corotto and Michel, 1998). Accommodation can result from a wide variety of physiological mechanisms. In many cases these mechanisms cause an outward current to develop slowly during a spike train, and it is this hyperpolarizing influence that causes spike frequency to decrease. After removal of the depolarizing stimulus, the outward currents generally persist and are manifested as an AHP.

The discovery of Ca^{2+}-activated K^+ currents (Meech, 1978; Latorre et al., 1989) provided a mechanism by which impulse activity can be controlled through feedback from the impulses themselves; the occurrence of an impulse increases intracellular calcium, which activates Ca^{2+}-activated K^+ currents to prolong the subsequent ISI. The participation of Ca^{2+} influx and Ca^{2+}-activated K^+ currents previously has been invoked to account for intermittent bursting behavior in Aplysia (Gorman and Thomas, 1978; Adams et al., 1980) and vertebrate neurons (Yarom et al., 1985; Hille, 1992; Fohlmeister and Miller, 1997).

In the present study, bath application of Co^{2+}, charybdotoxin, and iberiotoxin reduced AHPs and spike frequency accommodation in ORCs during injection of current steps of low and intermediate intensities. Thus, under these conditions Ca^{2+}-activated K^+ currents are responsible for generation of AHPs and spike frequency accommodation in the ORCs. The occurrence of an impulse in ORCs increases the concentration of intracellular calcium, which activates Ca^{2+}-activated K^+ currents to induce spike frequency accommodation in ORCs. After the termination of the depolarizing stimulus, the Ca^{2+}-activated K^+ currents are manifest as an AHP. This mechanism underlying the AHP and spike frequency accommodation in the ORCs is quite similar to that in CNS neurons (Yarom et al., 1985; Fohlmeister and Miller, 1997; Chitwood and Jaffe, 1998). A similar mechanism of AHPs is also reported in lobster ORCs, however the mechanism underlying spike frequency accommodation remained uncertain (Corotto and Michel, 1998).

In addition to Ca^{2+}-activated K^+ currents, AHPs in lobster ORCs are also regulated by two other mechanisms that occur when the ORCs are depolarized: deactivation of *h* currents and activation of a tiny K^+ current that does not require an influx of Ca^{2+} (Corotto and Michel, 1998). In lobster ORCs, *h* currents are likely to be active at rest, where they provide a constant, depolarizing influence. Further depolarization deactivates *h* currents, allowing the ORC to be briefly hyperpolarized when that depolarizing influence is removed, thus generating AHPs. By contrast, in newt ORCs hyperpolarizing voltage steps induced no inward current, suggesting that newt ORCs do not express *h* currents. In addition, 100 nM charybdotoxin, 50 nM iberiotoxin, and 1 mM $CoCl_2$ almost completely blocked the AHP (Fig. 1 *C*), but 2 mM CsCl did not significantly change the AHP (Fig. 1 *E*). These results indicate that AHPs in newt ORCs are generated by Ca^{2+}-activated K^+ currents rather than by *h* currents or Ca^{2+}-insensitive currents.

Because newt ORCs express not only L-type Ca^{2+} channels but also T-type Ca^{2+} channels, which contribute to lower the threshold of spike generation (Kawai et al., 1996), bath application of 1 mM Co^{2+}, the nonspecific blocker of voltage-gated Ca^{2+} channels, blocks both types of Ca^{2+} channels in the ORCs. It is still unclear how many Ca^{2+}-activated K^+ channels are activated by an influx of Ca^{2+} through the T-type Ca^{2+} channels. However, the I-V relationship of the Ca^{2+}-activated K^+ currents was quite similar to that of the L-type Ca^{2+} currents (Fig. 7). It is likely that Ca^{2+} influx through L-type Ca^{2+} channels rather than T-type Ca^{2+} channels mainly gates the Ca^{2+}-activated K^+ channels. Thus, blockage by Co^{2+} of the L-type Ca^{2+} currents is mainly responsible for the inhibition of spike frequency accommodation.

The first ISI in charybdotoxin or in iberiotoxin was longer than under control conditions (Fig. 1, *D* and *F*). This mechanism remains uncertain. However, because charybdotoxin or iberiotoxin slightly depolarized the resting potentials of ORCs, the voltage-gated Na^+ channels under application of those agents should be slightly more inactivated than the Na^+ channels under control conditions. Thus, in the presence of charybdotoxin or iberiotoxin, a longer ISI between the first and the second spike may be required to reactivate the voltage-gated Na^+ channels than under control conditions.

Effects of inactivation of voltage-gated Na^+ currents on spike frequency accommodation

When a current step of high intensity is injected into ORCs, inactivation of voltage-gated Na^+ currents is likely to be responsible for spike frequency accommodation in ORCs. Stimuli at high intensities (more than 12 pA) progressively reduced the spike amplitude (Fig. 2) and the spike frequency (Fig. 3 *C*, filled circles). A similar result is also observed in ORCs of other species (Trotier, 1994). A stimulation at high intensities ($>$10 pA) leads to a progressive and sometimes complete decline in action potentials of salamander and frog ORCs (Trotier and MacLeod, 1983; Trotier, 1994), which has been suggested to reflect progressive inactivation of voltage-gated Na^+ currents during the graded membrane depolarization. That is, the decrease by strong stimuli of the repolarization duration appears to change the spike generation markedly: the membrane potential is less repolarized and Na^+ channels are less effectively reactivated; the im-

pulse amplitude is lower and consequently voltage-gated K^+ channels are less activated; finally the firing ceases and only an oscillating membrane potential is recorded.

In the present experiment spike frequency accommodation was observed even in the presence of charybdotoxin at a strong stimulation (Fig. 2 *B*), suggesting that some current other than the Ca^{2+}-activated K^+ currents is involved in spike frequency accommodation at strong stimulations. Because inactivation of voltage-gated Na^+ currents is strongly voltage dependent, it is important to know how many Na^+ channels are available during the graded depolarization to understand their contribution to action potential generation. Because the inactivation curve for voltage-gated Na^+ currents in newt ORCs is fitted by a single Boltzmann function (figure 7 *B* in Kawai et al., 1996), the fraction of Na^+ channels to be activated during the graded depolarization (from ~ -40 mV to ~ -30 mV; see Fig. 2) can be estimated from the following function.

$$1/(1 + \exp((V - V_{\text{half}})/K_{\text{h}}))$$

in which V represents the membrane potential, V_{half} represents the half-inactivation voltage, and K_{h} represents a coefficient. V_{half} was -53 mV and K_{h} was 7.8 mV (Kawai et al., 1996). At those membrane potentials (from ~ -40 mV to ~ -30 mV) only 5 to 16% of Na^+ channels are available to generate action potentials. Thus, at strong stimuli it is likely that inactivation of voltage-gated Na^+ currents, not Ca^{2+}-activated K^+ currents, is mainly responsible for spike frequency accommodation in ORCs.

Although in the presence of charybdotoxin there was still a slight decline in the firing rate after the stimulus onset at low and intermediate stimuli (<12 pA; Fig. 1 *C*), spike frequency accommodation was markedly reduced by charybdotoxin and iberiotoxin. This suggests that at low and intermediate stimuli the Ca^{2+}-activated K^+ currents are mainly responsible for spike frequency accommodation in ORCs rather than inactivation of voltage-gated Na^+ currents. However, the slight decline in the firing rate in the presence of charybdotoxin (Fig. 1 *C*) is likely to be due to inactivation of voltage-gated Na^+ currents.

Spike frequency adaptation in ORCs

In newt ORCs a conditioning stimulus with the current step and the odorant-induced current markedly shifted the response range of action potentials induced by the same test stimulus to higher intensities, indicating spike frequency adaptation and odor adaptation in ORCs, respectively. A similar phenomenon is reported in frog ORCs using the suction pipette technique (Reisert and Matthews, 1999). They showed that exposure of ORCs to an adapting prepulse odorant stimulation resulted in a progressive shift of the response range of the spiking frequency (Reisert and Matthews, 1999). In their experiments, however, the mechanism underlying the displacement of the response range remained unclear.

In the present experiments the dynamic patch-clamp recording technique was used to examine selectively the effects of the somatic currents on odor adaptation in intact ORCs. Bath application of 100 nM charybdotoxin and 50 nM iberiotoxin blocked the shift of the response range of the spiking frequency (Fig. 5 *F*). A similar result was obtained in the response range of the spikes generated by injection of current steps (Fig. 3 *D*). Therefore, I suggest that the somatic Ca^{2+}-activated K^+ currents can regulate odor adaptation of ORCs by modulating their spike encoding.

Comparison of odor adaptation at the ciliary level with the somatic level

Mechanisms underlying odor adaptation at the ciliary membrane of ORCs have been intensively investigated (Bakalyar and Reed, 1991; Breer and Boekhoff, 1992; Ronnett and Snyder, 1992; Firestein, 1992; Kurahashi and Yau, 1994; Schild and Restrepo, 1998). Several mechanisms by which Ca^{2+} can evoke an adaptive response have already been proposed, varying from inhibition of cAMP production (Sklar et al., 1986) or stimulation of cAMP hydrolysis (Borisy et al., 1992), to Ca^{2+}-mediated desensitization of the CNG channel (Liu et al., 1994; Kurahashi and Menini, 1997). Receptor-protein phosphorylation has also been shown to decrease the activity of adenylyl cyclase (Boekhoff and Breer, 1992), and this mechanism is not dependent on Ca^{2+}.

Kurahashi and Menini (1997) examined the effect of a pulse of odorant on the transduction current response that was evoked by a second pulse of the same odorant. They showed that the first conditioning stimulus decreased the response to the second stimulus in normal Ringer's solution, and the conditioning stimulus shifted the dose-response relationship to higher concentrations of the odorant. This indicates odor adaptation at the ciliary membrane of ORCs. They also analyzed recovery kinetics of the transduction current from odor adaptation, and its time for full recovery is ~ 7 s.

In the present experiment, I examined the kinetics of recovery from transduction current adaptation and spike frequency adaptation. The time course of recovery from the transduction current adaptation could be fitted by a single exponential function with a time constant of 3.7 s, and its time for full recovery was 8 to 10 s (Fig. 4). This value is similar to the previous report (Kurahashi and Menini, 1997). In contrast, the time course of recovery from spike frequency adaptation could be fitted with a short time constant of 0.51 s, and its time for full recovery was ~ 2 s (Fig. 4 *B*). This suggests that the somatic adaptational mechanism through the Ca^{2+}-activated K^+ currents (spike frequency adaptation) contributes to odor adaptation in ORCs only for a short period compared with the ciliary adaptational mech-

anism. That is, within ~1 s after the first conditioning odorant pulse onset, both the somatic and ciliary adaptational mechanism regulate odor adaptation in ORCs. In contrast, ~1 s after the conditioning pulse, only the ciliary adaptational mechanism plays a dominant role in odor adaptation. Therefore, the somatic Ca^{2+}-activated K^+ currents contribute to enhancing odor adaptation only for ~1 s after odorant stimuli by modulating spike encoding of ORCs.

I thank Dr. E.-I. Miyachi, A. Kaneko, and T. Kurahashi for their advice. This work was supported by Japan Society of the Promotion of Science Number 12780620, the SKYLARK Food Science Institute, the Fujisawa Foundation, Narishige Neuroscience Research Foundation, and the Research Foundation for Pharmaceutical Sciences.

REFERENCES

Adams, P. R., S. J. Smith, and S. H. Thompson. 1980. Ionic currents in molluscan soma. *Annu. Rev. Neurosci.* 3:141–167.

Amerine, M. A. 1965. Principles of Sensory Evaluation of Food. Academic Press, New York. 186–186.

Bakalyar, H. A., and R. R. Reed. 1991. The second messenger cascade in olfactory receptor neurons. *Curr. Biol.*1:204–208.

Boekhoff, I., and H. Breer. 1992. Termination of second messenger signaling in olfaction. *Proc. Natl. Acad. Sci. U. S. A.* 89:471–474.

Borisy, F. F., G. V. Ronnett, A. M. Cunningham, D. Juilfs, J. Beavo, and S. H. Snyder. 1992. Calcium/calmodulin-activated phosphodiesterase expressed in olfactory receptor neurons. *J. Neurosci.* 12:915–923.

Breer, H., and I. Boekhoff. 1992. Second messenger signaling in olfaction. *Curr. Biol.* 2:439–443.

Candia, S., M. L. Garcia, and R. Latorre. 1992. Mode of action of iberiotoxin, a potent blocker of the large conductance Ca^{2+} -activated K^+ channel. *Biophys. J.* 63:583–590.

Chitwood, R. A., and D. B. Jaffe. 1998. Calcium-dependent spike-frequency accommodation in hippocampal CA3 nonpyramidal neurons. *J. Neurophysiol.* 80:983–988.

Corotto, F. S., and W. C. Michel. 1998. Mechanisms of after hyperpolarization in lobster olfactory receptor neurons. *J. Neurophysiol.* 80: 1268–1276.

Corotto, F. S., D. R. Piper, N. Chen, and W. C. Michel. 1996. Voltage- and Ca^{2+}-gated currents in zebrafish olfactory receptor neurons. *J. Exp. Biol.* 199:1115–1126.

Delgado, R., and P. Labarca. 1993. Properties of whole cell currents in isolated olfactory neurons from the chilean toad *Caudiverbera caudiverbera. Am. J. Physiol.* 264:C1418–C1427.

Duchamp-Viret, P., M. A. Chaput, and A. Duchamp. 1999. Odor response properties of rat olfactory receptor neurons. *Science.* 25:2171–2174.

Fan, J. S., and P. Palade. 1998. Perforated patch recording with beta-escin. *Pflügers Arch.* 436:1021–1023.

Firestein, S. 1992. Electrical signals in olfactory transduction. *Curr. Biol.* 2:444–448.

Firestein, S., C. Picco, and A. Menini. 1993. The relation between stimulus and response in olfactory receptor cells of the tiger salamander. *J. Physiol.* 468:1–10.

Firestein, S., and F. S. Werblin. 1987. Gating currents in isolated olfactory receptor neurons of the larval tiger salamander. *Proc. Natl. Acad. Sci. U. S. A.* 88:6292–6296.

Fohlmeister, J. F., and R. F. Miller. 1997. Impulse encoding mechanisms of ganglion cells in the tiger salamander retina. *J. Neurophysiol.* 78: 1935–1947.

Frings, S., and B. Lindemann. 1990. Single unit recording from olfactory cilia. *Biophys. J.* 57:1091–1094.

Gorman, A. L., and M. V. Thomas. 1978. Changes in the intracellular concentration of free calcium ions in a pacemaker neurone, measured with the metallochromic indicator dye arsenazo III. *J. Physiol.* 275: 357–376.

Hille, B. 1992. Potassium channels and chloride channels. *In* Ionic Channels of Excitable Membranes. B. Hille, editor. Sinauer Associates, Sunderland, MA. 115–139.

Kawai, F., T. Kurahashi, and A. Kaneko. 1996. T-type Ca^{2+} channel lowers the threshold of spike generation in the newt olfactory receptor cell. *J. Gen. Physiol.* 108:525–535.

Kawai, F., T. Kurahashi, and A. Kaneko. 1997. Nonselective suppression of voltage-gated currents by odorants in the newt olfactory receptor cells. *J. Gen. Physiol.* 109:265–272.

Kawai, F., T. Kurahashi, and A. Kaneko. 1999. Adrenaline enhances odorant contrast by modulating signal encoding in olfactory receptor cells. *Nat. Neurosci.* 2:133–138.

Kawai, F., and E.-I. Miyachi. 2001. Enhancement by T-type Ca^{2+} currents of odor sensitivity in olfactory receptor cells. *J. Neurosci.* 21:1–5.

Kleene, S. J. 1993. Origin of the chloride current in olfactory transduction. *Neuron.* 11:123–132.

Kurahashi, T., and A. Kaneko. 1993. Gating properties of the cAMP-gated channel in toad olfactory receptor cells. *J. Physiol.* 466:287–302.

Kurahashi, T., and A. Menini. 1997. Mechanism of odorant adaptation in the olfactory receptor cell. *Nature.* 385:725–729.

Kurahashi, T., and K.-W. Yau. 1994. Tale of an unusual chloride current. *Curr. Biol.* 4:256–258.

Kusaka, S., N. Kapousta-Bruneau, D. G. Green, and D. G. Puro. 1998. Serum-induced changes in the physiology of mammalian retinal glial cells: role of lysophosphatidic acid. *J. Physiol.* 506:445–458.

Latorre, R., A. Oberhauser, P. Labarca, and O. Alvarez. 1989. Varieties of calcium-activated potassium channels. *Annu. Rev. Physiol.* 51:385–399.

Liu, M., T. Y. Chen, B. Ahamed, J. Li, and K.-W. Yau. 1994. Calcium-calmodulin modulation of the olfactory cyclic nucleotide-gated cation channel. *Science.* 266:1348–1354.

Lucero, M. T., and N. Chen. 1997. Characterization of voltage- and Ca^{2+}-activated K^+ channels in squid olfactory receptor neurons. *J. Exp. Biol.* 200:1571–1586.

Lynch, J. W., and P. H. Barry. 1991. Inward rectification in rat olfactory receptor neurons. *Proc. R. Soc. Lond. B. Biol. Sci.* 243:149–153.

Maue, R. A., and V. E. Dionne. 1987. Patch-clamp studies of isolated mouse olfactory receptor neurons. *J. Gen. Physiol.* 90:95–125.

McCormick, D. A., and H. C. Pape. 1990. Properties of a hyperpolarization-activated cation current and its role in rhythmic oscillation in thalamic relay neurones. *J. Physiol.* 431:291–318.

Meech, R. W. 1978. Calcium-dependent potassium activation in nervous tissues. *Annu. Rev. Biophys. Bioeng.* 7:1–18.

Miyamoto, T., D. Restrepo, and J. H. Teeter. 1992. Voltage-dependent and odorant-regulated currents in isolated olfactory receptor neurons of the channel catfish. *J. Gen. Physiol.* 99:505–530.

Nakamura, T., and G. H. Gold. 1987. A cyclic nucleotide-gated conductance in olfactory receptor cilia. *Nature.* 325:442–444.

Nevitt, G. A., and W. J. Moody. 1992. An electrophysiological characterization of ciliated olfactory receptor cells of the coho salmon *Oncorhynchus kisutch. J. Exp. Biol.* 166:1–17.

Puro, D. G., and E. L. Stuenkel. 1995. Thrombin-induced inhibition of potassium currents in human retinal glial (Muller) cells. *J. Physiol.* 485:337–348.

Reisert, J., and H. R. Matthews. 1999. Adaptation of the odour-induced response in frog olfactory receptor cells. *J. Physiol.* 15:801–813.

Restrepo, D., J. H. Teeter, and D. Schild. 1996. Second messenger signaling in olfactory transduction. *J. Neurobiol.* 30:37–48.

Ronnett, G. V., and S. H. Snyder. 1992. Molecular messengers of olfaction. *Trends Neurosci.* 15:508–513.

Schild, D. 1989. Whole-cell currents in olfactory receptor cells of *Xenopus laevis. Exp. Brain Res.* 78:223–232.

Schild, D., and D. Restrepo. 1998. Transduction mechanisms in vertebrate olfactory receptor cells. *Physiol. Rev.* 78:429–466.

Sklar, P. B., R. R. Anholt, and S. H. Snyder. 1986. The odorant-sensitive adenylate cyclase of olfactory receptor cells: differential stimulation by distinct classes of odorants. *J. Biol. Chem.* 261:15538–15543.

Torre, V., J. F. Ashmore, T. D. Lamb, and A. Menini. 1995. Transduction and adaptation in sensory receptor cells. *J. Neurosci.* 15:7757–7768.

Trotier, D. 1986. A patch-clamp analysis of membrane currents in salamander olfactory receptor cells. *Pflügers Arch.* 407:589–595.

Trotier, D. 1994. Intensity coding in olfactory receptor cells. *Semin. Cell. Biol.* 519:47–54.

Trotier, D., and P. MacLeod. 1983. Intracellular recordings from salamander olfactory receptor cells. *Brain Res.* 268:225–237.

Womble, M. D., and H. C. Moises. 1993. Hyperpolarization-activated currents in neurons of the rat basolateral amygdala. *J. Neurophysiol.* 70:2056–2065.

Yarom, Y., M. Sugimori, and R. Llinas. 1985. Ionic currents and firing patterns of mammalian vagal motoneurons. *J. Neurosci.* 16:719–737.

Zufall, F., and T. Leinders-Zufall. 2000. The cellular and molecular basis of odor adaptation. *Chem. Senses.* 25:473–481.

Zufall, F., M. Stengl, C. Franke, J. G. Hildebrand, and H. Hatt. 1991. Ionic currents of cultured olfactory receptor neurons from antennae of male *Manduca sexta. J. Neurosci.* 11:956–965.